

# InfoDisent: Explainability of Image Classification Models by Information Disentanglement

Łukasz Struski, Jacek Tabor

Faculty of Mathematics and Computer Science  
Jagiellonian University, Kraków, Poland

lukasz.struski@uj.edu.pl, jacek.tabor@uj.edu.pl

## Abstract

Understanding the decisions made by image classification networks is a critical area of research in deep learning. This task is traditionally divided into two distinct approaches: post-hoc methods and intrinsic methods. Post-hoc methods, such as GradCam, aim to interpret the decisions of pre-trained models by identifying regions of the image where the network focuses its attention. However, these methods provide only a high-level overview, making it difficult to fully understand the network’s decision-making process. Conversely, intrinsic methods, like prototypical parts models, offer a more detailed understanding of network predictions but are constrained by specific architectures, training methods, and datasets.

In this paper, we introduce InfoDisent, a hybrid model that combines the advantages of both approaches. By utilizing an information bottleneck, InfoDisent disentangles the information in the final layer of a pre-trained deep network, enabling the breakdown of classification decisions into basic, understandable atomic components. Unlike standard prototypical parts approaches, InfoDisent can interpret the decisions of pre-trained classification networks and be used for making classification decisions, similar to intrinsic models. We validate the effectiveness of InfoDisent on benchmark datasets such as ImageNet, CUB-200-2011, Stanford Cars, and Stanford Dogs for both convolutional and transformer backbones.

## Introduction and related works

Machine learning techniques, such as deep neural networks, have become essential tools in various applications including classification, image generation, speech recognition, and natural language processing. These techniques have achieved remarkable effectiveness, often rivaling human capabilities and sometimes surpassing them. A significant recent development in deep learning is the focus on model interpretability, giving rise to a subfield of artificial intelligence known as eXplainable AI (XAI) (Xu et al. 2019). Interpreting and understanding model learning is crucial in critical applications such as medicine, image recognition, autonomous driving, etc (Struski et al. 2024; Khan et al. 2001; Bojarski et al. 2017; Samek et al. 2021; Nauta et al. 2023b; Patrício, Neves, and Teixeira 2023).

Historically, the world of XAI is divided into two disjoint categories: post-hoc interpretability (Ribeiro, Singh, and Guestrin 2016; Lundberg and Lee 2017; Selvaraju et al. 2017), where we analyze the pre-trained model to explain

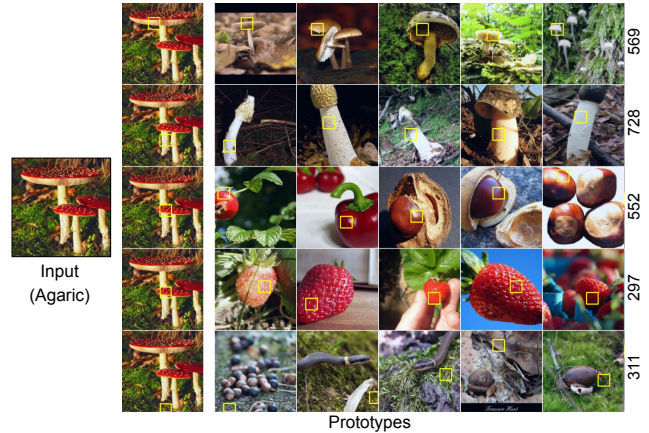


Figure 1: Decision explanation constructed by InfoDisent for the pre-trained ViT (Dosovitskiy et al. 2020) feature space on the Agaric mushrooms image from the ImageNet dataset (left). In the prototype block (right) each row represents the prototypes (the corresponding channel number is on the right side of the block). The yellow boxes in each row show the activation of a given prototype, while in the first column, we show the activation of corresponding prototypes in the original image. Observe that we can informally trace the decision of ViT behind assigning the class Agaric to the image on the left to having a hat (channel 569), a white leg (channel 728), a reddish shine (channel 552), a strawberry texture (channel 297) and the appearance of ground with moss (channel 311).

its predictions, and inherently explained models (Chen et al. 2019; Böhle, Fritz, and Schiele 2022), where the aim lies in building networks which decisions are easy to interpret. Both of the above approaches have their advantages and disadvantages.

**Post-hoc methods** In the post-hoc methods, we interpret existing pre-trained network architectures. The commonly used methods like SHAP (Shapley 1951; Lundberg and Lee 2017), LIME (Ribeiro, Singh, and Guestrin 2016), LRP (Bach et al. 2015) or Grad-CAM (Selvaraju et al. 2017) provide in practice only feature importance which can be visualized as a saliency map that shows on which part of the

image the model has focused its attention. This allows us to check if the model does not focus its attention outside of the object of interest (Ribeiro, Singh, and Guestrin 2016), however, it is in general not sufficient to really understand the reasons behind given predictions. Additionally, post hoc methods allow typically only local explanations (per the prediction of a given image), and do not allow to understand of the prerequisites to the given class.

**Inherently explained models** While post-hoc methods are easy to implement due to their non-intrusive nature, they often produce biased and unreliable explanations (Adebayo et al. 2018). To address this, recent research has increasingly focused on designing self-explainable models that make the decision process directly visible (Brendel and Bethge 2019; Alvarez Melis and Jaakkola 2018). Many of these interpretable solutions utilize attention mechanisms (Liu et al. 2021; Zheng et al. 2019) or exploit the activation space, such as with adversarial autoencoders (Guidotti et al. 2020). Among the most recent approaches, ProtoPNet (Chen et al. 2019) has significantly influenced the development of self-explainable models. It learns class-specific prototypes, similar to concepts, with a fixed number per class. The model classifies inputs by calculating responses from each class’s prototypes and summarizing these responses through a fully connected layer, providing explanations as a weighted sum of all prototypes. This method inspired the development of several other self-explainable models (Donnelly, Barnett, and Chen 2022; Rymarczyk et al. 2021, 2022; Wang et al. 2021; Nauta et al. 2023a; Donnelly, Barnett, and Chen 2022; Wang et al. 2021). Typically, in the prototypical parts model, the final decision of a given class is decomposed into the appearance of a few selected prototypes, which are similar to some strongly localized parts of some chosen images from the dataset. We see that in this approach the final class decision is split into a set of simpler and interpretable compounds.

Although intrinsic methods, like prototypical parts models, offer a more detailed understanding of network predictions as compared to post-hoc methods, they are constrained to specific architectures, training methods, and datasets<sup>1</sup>.

**InfoDisent** Thus in our opinion, one of the most important problems in XAI is whether it is possible to construct Post-hoc methods that would provide similar functionality to inherently interpretable ones. In particular, similarly to prototypical models, we would like to be able to split the final decisions into simpler interpretable components. Additionally, the ability to explain global predictions (what are the reasons for choosing a given class in general) is extremely desirable.

In this paper, we propose a hybrid model InfoDisent, whose aim is to take the best from both worlds and provide a partial positive answer to the above problem. The motivation of InfoDisent was to add the functionality of proto-

<sup>1</sup>In particular prototypical parts methods work well if the dataset consists of classes which are variations of objects of similar shape (like birds or cars), and consequently typically do not obtain a good prediction on diverse datasets like ImageNet.

typical models to pre-trained architectures (we test InfoDisent both on convolutional and transformer architectures). To do so InfoDisent disentangles the information from the feature layer into separate prototype channels (similarly to the prototype-based model PIP-Net (Nauta et al. 2023a)). This is achieved by applying the information bottleneck, where we encourage the sparsity of the activation of a given prototype channel. Consequently, InfoDisent constructs interpretations of feature space of pre-trained models, which allow the decomposition of the final decision into simpler atomic components. Consequently, we can explain the decision behind a given class by looking at the most active prototype channels, see Figure 1.

Summarizing, the contributions of the paper are the following:

- we propose InfoDisent, a hybrid model devoted to explainability, which lies in the border between Post-hoc and intrinsic models,
- InfoDisent has similar applicability to prototypical parts models, but constructs interpretations for feature space of pre-trained networks,
- the final class decision of InfoDisent can be traced back to easily interpretable prototypical channels.

### InfoDisent: architecture

Our motivation comes from the general methodology of prototypical models, which can be described in the following way:

- trace the final class decision to the co-occurrence in the image of some prototypes,
- each prototype can be visualized by some prototypes from the training dataset,
- prototypes should be strongly localized parts of the image.

We claim that even for pre-trained models it is possible to disentangle the channels in the feature space in such a way that they will become sufficiently informative to satisfy the above points. In InfoDisent we disentangle the channels in feature space by applying an orthogonal map in the pixel space, and consequently do not change the inner-lying distance and scalar product.

Since we disentangle the channels in the feature space, we restrict our attention to images in the feature space and consider only the classification head. Thus consider the data set of images in the feature space, which consists of images of possibly different resolutions but the same number of channels  $d$ .

**Default classification head in deep networks** To establish notation, let us first describe the typical classification head. In the case of a classification task with  $k$  classes, we apply the following operations for the image  $I$  in the feature space:

1.  $I \rightarrow v_I = \text{avg\_pool\_over\_channels}(I) \in \mathbb{R}^d$
2.  $v_I \rightarrow w_I = Av_I$ , where  $A$  is a matrix of dimensions  $d \times k$
3.  $w_I \rightarrow p_I = \text{softmax}(w_I)$ .

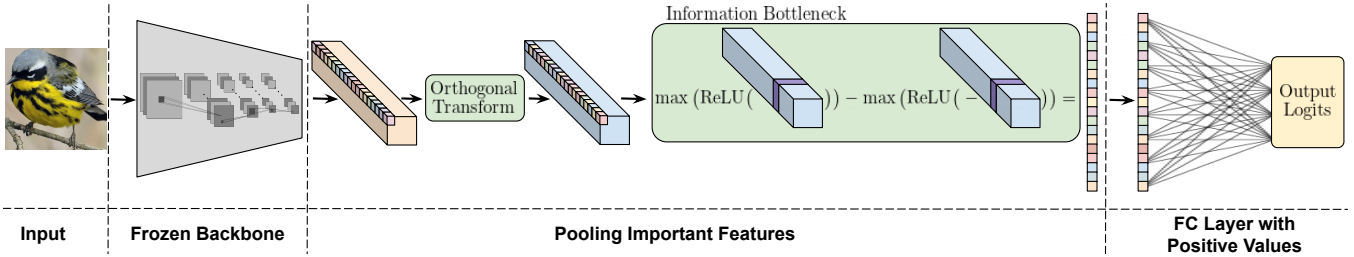


Figure 2: Our image classification interpretation model, InfoDisent, features three main components: a pre-trained backbone, a pooling layer for key features, and a fully connected layer. The CNN/transformer backbone, with frozen weights, is not further trained. The pooling layer extracts features from the last transformer or convolutional layer and identifies key positive and negative features. These are then combined into a dense vector, which is processed by a fully connected linear layer with nonnegative entries in the final stage.

In the case of InfoDisent we apply a few mechanisms to ensure the desired properties. First, we need to be able to disentangle the channel space. To do so we apply the unitary map  $U$  in the pixel space. Next, we apply the information bottleneck – for a given channel instead of the average pool where all pixels participate, we use extremely sparse analog where only the value of the highest positive and negative pixels are used. Finally, as is common in interpretable methods we use matrix  $A$ , but only with nonnegative coefficients to allow only positive reasoning.

**The sparse pooling features mechanism** Most interpretable models involve retraining certain parts of the CNN (Chen et al. 2019; Rymarczyk et al. 2022), whereas others, like PIP-Net (Nauta et al. 2023a), retrain the entire CNN. In contrast, our method utilizes a pre-trained CNN or transformer without further modification during training. We first employ a trainable orthogonal transformation  $U$  on pixel space to enable the disentanglement of hidden features from feature maps<sup>2</sup>. To enforce the disentanglement we follow by an introduced sparse analogue of average pooling over channel  $K$  given by

$$K \rightarrow \text{mx\_pool}(K) = \max(\text{ReLU}(K)) - \max(\text{ReLU}(-K)).$$

Observe that to compute  $\text{mx\_pool}(K)$  we need to know only the highest positive and negative pixel values of  $K$ , contrary to  $\text{avg\_pool}$ , where all the pixel values are needed. Subsequently, we identify sparse representations (superpixels) within the channels that contribute positively or negatively to predictions. This enables us to generate heatmaps akin to Grad-CAM (Selvaraju et al. 2017) without necessitating a backward model step, as shown in Figure 5a. Importantly, unlike Grad-CAM, our technique supports the visualization of negative heatmaps, resembling the LRP (Bach et al. 2015) method that requires a backward pass in a neural network. Our method operates solely during the forward step.

<sup>2</sup>To parametrize orthogonal maps, we restrict to those with positive determinants and use the formula  $U = \exp(W - W^T)$ , where  $\exp(\cdot)$  denote the matrix exponential (Hall and Hall 2013). We utilize the fact that the space of orthogonal matrices with positive determinants coincide with exponentials of skew-symmetric matrices (Shepard, Brozell, and Gidofalvi 2015).

Finally, as is common in XAI models, to allow only positive reasoning we allow the matrix  $A$  to have only nonnegative values.

**Classification head in InfoDisent** Finally, the classification head in InfoDisent is given by:

1.  $I = (I_{rs})_{rs} \rightarrow J = (UI_{rs})$ , where  $U : \mathbb{R}^d \rightarrow \mathbb{R}^d$  is an orthogonal matrix and  $I_{rs}$  denotes the pixel value of  $I$  with coordinates  $r$  and  $s$ ,
2.  $J \rightarrow v_J = \text{mx\_pool\_over\_channels}(J) \in \mathbb{R}^d$ , where for a given channel  $K$  we have
$$\text{mx\_pool}(K) = \max(\text{ReLU}(K)) - \max(\text{ReLU}(-K)),$$
3.  $v_J \rightarrow w_J = Av_J$ , where  $A$  is a matrix with nonnegative coefficients of dimensions  $d \times k$
4.  $w_J \rightarrow p_I = \text{softmax}(w_J)$

**InfoDisent model** Thus InfoDisent consists of two main components: the frozen CNN or transformer Backbone, and InfoDisent classification head, as illustrated in Figure 2.

The first component, the CNN or transformer Backbone, is a frozen classical pre-trained network up to the final feature maps layer. Importantly, this part of the network and its weights remain unaltered during the training of InfoDisent, ensuring that the learned feature representations are preserved.

The second component involves pooling important features from the final feature maps produced by the Frozen Backbone. This pooling mechanism encourages the network to use information bottlenecks to build maximally informative channels independent of each other. This leads to constructing prototypical channels, which can be easily interpreted. The final element is the fully connected layer, which is distinguished by its positive weight values. This restriction on positivity, except biases handled as in conventional linear layers, ensures that the information about the positive or negative contributions of selected features from the previous part of the model is preserved. This constraint is beneficial for the interpretability of the model’s predictions, as it clarifies the contribution of each feature to the final output.

Observe, that contrary to some Post-hoc methods InfoDisent need training of the model on the whole dataset.

## Understanding the classification decisions

**Prototypes in InfoDisent** The crucial consequence of InfoDisent that is disentangles the channels making them interpretable. Thus, similarly to PiPNet (Nauta et al. 2023a), we identify channels as prototypes. To illustrate a given prototype channel, we present five images from the training dataset on which the activation of the channel is the greatest, see Figure 3, where we present consecutive prototypes for the pre-trained ResNet-50 model. This follows from the fact that for better interpretability of model decisions, it is beneficial for humans to be presented from 4 to 9 concepts (Rymarzyk et al. 2022). Formally, similarly as in prototypical models, as the prototypical part, we understand the part of the image corresponding to pixels in feature space with maximal activation, marked by the yellow box in Figure 3. Observe that the presented prototypes seem consistent with each other, and could be well interpreted.

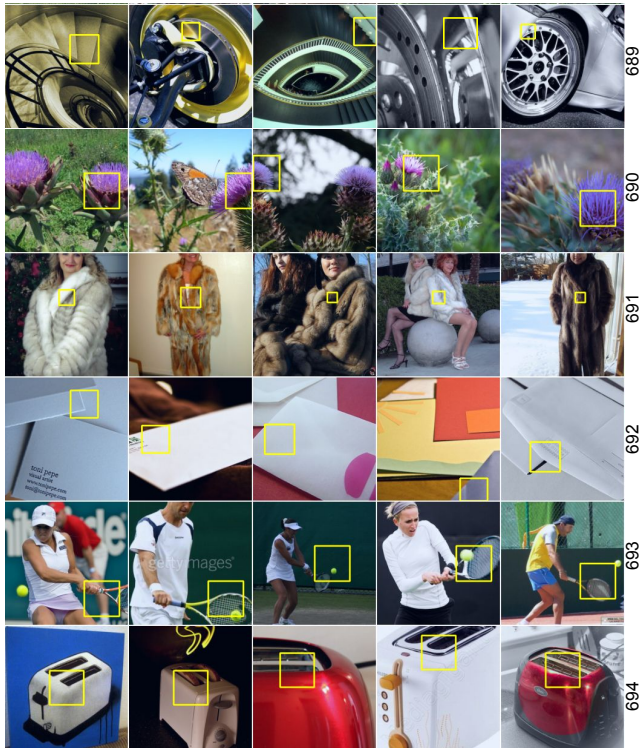


Figure 3: The image shows prototypes from channels 689 to 694 in a trained ResNet-50 model on the ImageNet dataset. Each row displays the 5 most significant prototypes from a single channel. The prototypes are highlighted in yellow boxes.

**Understanding the Decision for a Given Image by Prototypes** Now that we can understand and visualize prototypes, there appears to be a question of how to visualize the prototypes crucial for the decision of the model on the given image. To do this we chose 5 prototypical channels which

are most important for the prediction<sup>3</sup> in Figure 4. For each channel, we identified 5 images from the training dataset that exhibit the strongest activation values for that channel, as depicted by the red spots in Figure 5a. In simpler terms, we selected the top 5 images based on the highest activation values, or arg-top5, for each channel.

The model’s proposed prototypes are easy to interpret. Moreover, unlike current state-of-the-art prototype methods, our model excels at interpreting images from the ImageNet dataset. More examples from various datasets and models are presented in the Supplementary Materials.

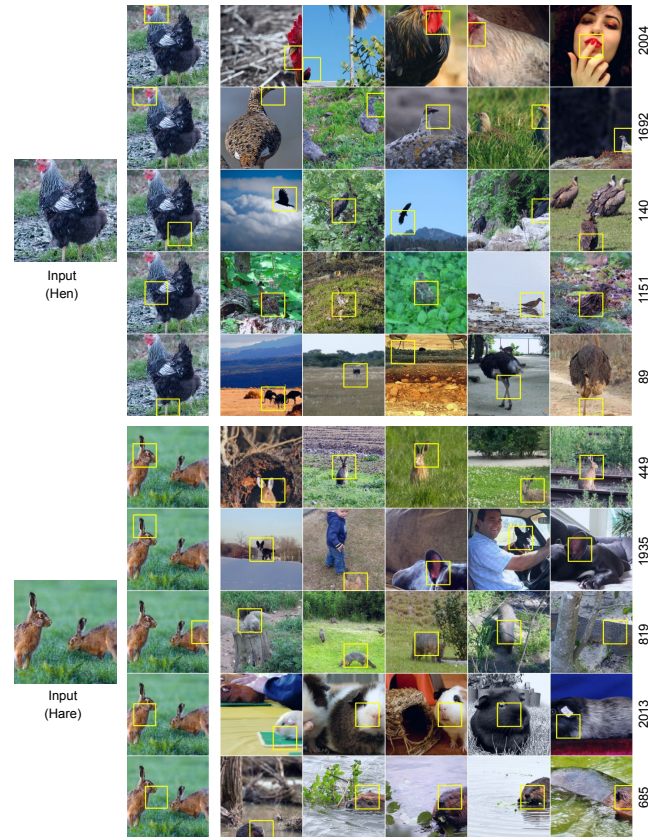
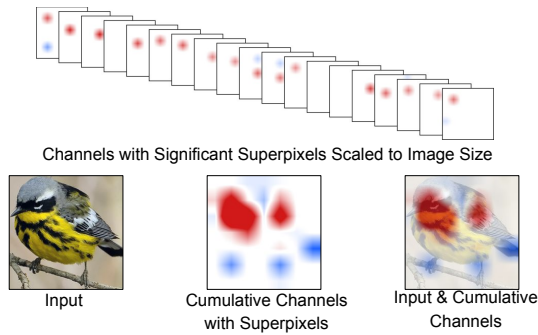


Figure 4: Sample examples illustrating how the ResNet-50 model, trained on the ImageNet dataset, explains the input images using prototypes.

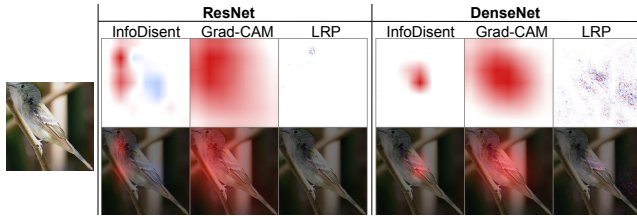
**Heatmaps** Our approach, which relies on representation channels, enables us to easily generate heatmaps similar to those produced by the Grad-CAM method, see Figure 5a. To do this we accumulate the activations of all prototypes (both positive and negative ones) over all channels. Since in InfoDisent we use information bottleneck, we obtain more localized results than other standard approaches.

Observe that, unlike Grad-CAM, our heatmaps also illustrate negative activations, akin to the Layer-Wise Relevance Propagation (LRP) method. While LRP can effectively highlight both positive and negative contributions to the model’s

<sup>3</sup>One can assume more subtle strategies, see Supplementary Materials.



(a) The top part shows a heatmap with positive (red) and negative (blue) sparse representations, each channel displaying one positive and one negative superpixel. These sparse representations are then aggregated and rescaled to the image size in the lower part.



(b) Example compares visual explanations from InfoDisent, Grad-CAM, and LRP. The left shows input images, with the following columns displaying explanations from these methods applied to ResNet and DenseNet.

Figure 5: The image demonstrates how to analyze and visualize decisions made by InfoDisent.

decision, it often faces challenges such as complexity in implementation and sensitivity to model architecture variations. Our method addresses these issues by providing clear and interpretable visualizations. Sample results using this explanation method are presented in Figure 5b.

**Understanding the Decision Behind Class** We examine the model’s decision-making process on a per-class basis by utilizing prototypes. To identify prototypes for a given class, we focus on key channels that are prominently activated across all test set images belonging to that class. These key channels are selected based on their consistent presence and strong activation in images of the same class. Once we have identified these crucial channels, we visualize the prototypes as previously described, providing a clear representation of what the model deems important for that particular class.

Figure 6 illustrates the prototypes for selected classes from the ImageNet dataset. Each prototype captures essential features such as material types, structural elements, or specific textures that are characteristic of the class.

## Experiments and Results

This section outlines the experiments conducted to compare our approach with current state-of-the-art methods, highlighting the most significant results. Our experiments utilized a variety of datasets, including well-established bench-

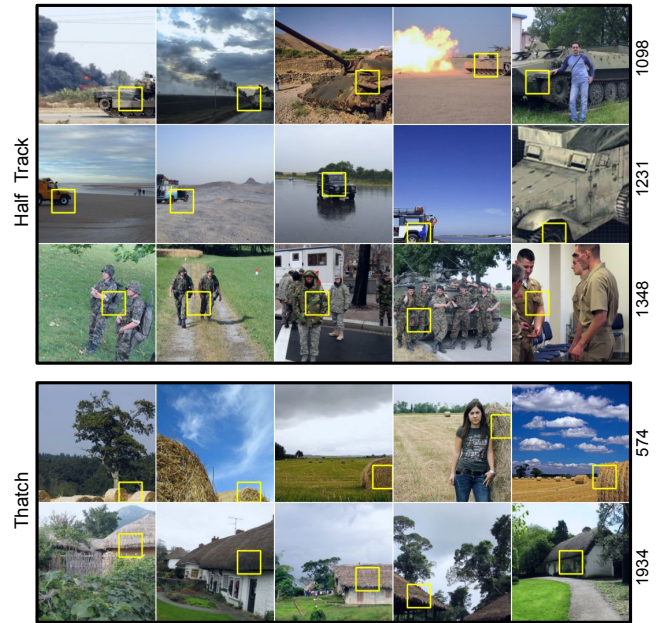


Figure 6: Prototypes of two classes (from top to bottom): Half Track and Thatch from the ImageNet dataset. Each row displays the 5 most significant prototypes for a specific channel, with the channel numbers listed on the right. The order of the prototypes within each row reflects their importance for explaining the given class. In the Half Track class, the prototypes from channel 1098 are the most crucial, followed by those from channels 1231 and 1348. These prototypes effectively explain the Half Track class, as they highlight elements of a tank (from channel 1098), a car, and the possible presence of soldiers on board.

marks for evaluating the explainability of artificial models: The Caltech-UCSD Birds-200-2011 (CUB-200-2011) (Wah et al. 2011), Stanford Cars (Krause et al. 2013), and Stanford Dogs (Khosla et al. 2011), as well as the newly introduced FunnyBirds (Hesse, Schaub-Meyer, and Roth 2023). Additionally, we incorporated the full ImageNet (Russakovsky et al. 2015) dataset for the first time in the class of prototypical networks.

Additional results and details concerning these experiments are provided in the Supplementary Materials.

## Classification Performance

To compare our approach, we selected several state-of-the-art, interpretable models based on the same CNN architectures as our approach. We categorized the models into a few groups based on their CNN architecture – ResNet-34/50 (He et al. 2016), DenseNet-121 (Huang et al. 2017), and ConvNeXt-Tiny (Liu et al. 2022b) – and the experiments we conducted on these datasets. Specifically, we performed two experiments: the first used cropped images for training and testing, and the second used full images.

In the first experiment, we utilized two key datasets: CUB-200-2011 and Stanford Cars, which are frequently employed in prototype model evaluations. We trained both the

Model	Dataset		
	CUB-200-2011	Cars	
<i>ResNet-34</i>	ResNet-34	82.4%	92.6%
	↳ InfoDisent (ours)	<b>83.5%</b>	<b>92.8%</b>
	-----	-----	-----
	ProtoPNet	79.2%	86.1%
	ProtoPShare	74.7%	86.4%
	ProtoPool	80.3%	89.3%
	ST-ProtoPNet	<b>83.5%</b>	91.4%
TesNet	82.7%	90.9%	
<i>ResNet-50</i>	ResNet-50	83.2%	93.1%
	↳ InfoDisent (ours)	<b>83.0%</b>	<b>92.9%</b>
	-----	-----	-----
	ProtoPool	–	88.9%
	ProtoTree	–	86.6%
PIP-Net	82.0%	86.5%	
<i>DenseNet-121</i>	DenseNet-121	81.8%	92.1%
	↳ InfoDisent (ours)	82.6%	<b>92.7%</b>
	-----	-----	-----
	ProtoPNet	79.2%	86.8%
	ProtoPShare	74.7%	84.8%
	ProtoPool	73.6%	86.4%
	ST-ProtoPNet	<b>85.4%</b>	92.3%
TesNet	84.8%	92.0%	
<i>ConvNeXt</i>	ConvNeXt-Tiny	83.8%	91.0%
	↳ InfoDisent (ours)	84.1%	<b>90.2%</b>
	-----	-----	-----
PIP-Net	<b>84.3%</b>	88.2%	

Table 1: Accuracy comparison of interpretability models using standard CNN architectures (utilized in explainable models) trained on cropped bird images of CUB-200-2011, and Stanford Cars (Cars). Our approach demonstrates superior performance across nearly all the datasets and models considered. For each dataset and backbone, we boldface the best result in the class of interpretable models.

base models and our models on these cropped images, with the results shown in Table 1. In the second experiment, we used CUB-200-2011 and Stanford Dogs datasets, but this time with the full images. The results of this experiment are detailed in Table 2.

In both experiments, our approach consistently outperformed the compared models. Additionally, training competitive methods often proves to be more challenging, requiring substantial computational resources and time due to the complex training processes involved. In contrast, our method simplifies this by only training the last two parts of the model network, with the CNN backbone remaining unchanged, thereby reducing the training effort and complexity.

In the next experiment in this part, we utilized the full ImageNet dataset and evaluated both traditional CNN models – such as ResNet-34/50, DenseNet-121, and ConvNeXt-Large – and popular transformer models, including VisionTransformer (ViT-B/16) (Dosovitskiy et al. 2020), SwinTransformer (Swin-S) (Liu et al. 2022a), and MaxVit (Tu et al.

Model	Dataset		
	CUB-200-2011	Dogs	
<i>ResNet-34</i>	ResNet-34	76.0%	84.5%
	↳ InfoDisent (ours)	<b>78.3%</b>	<b>83.9%</b>
	-----	-----	-----
	ProtoPNet	74.1%	76.1%
	ST-ProtoPNet	78.2%	83.4%
TesNet	76.5%	81.2%	
<i>ResNet-50</i>	ResNet-50	78.7%	87.4%
	↳ InfoDisent (ours)	79.5%	<b>86.6%</b>
	-----	-----	-----
	ProtoPNet	84.8%	78.1%
ST-ProtoPNet	<b>88.0%</b>	83.3%	
TesNet	87.3%	85.7%	
<i>DenseNet-121</i>	DenseNet-121	78.2%	84.1%
	↳ InfoDisent (ours)	80.6%	<b>83.8%</b>
	-----	-----	-----
	ProtoPNet	76.6%	75.4%
ST-ProtoPNet	<b>81.8%</b>	82.9%	
TesNet	80.9%	82.1%	

Table 2: Classification accuracy on full CUB-200-2011, and Stanford Dogs datasets by competing approaches using different CNN backbones. For each dataset and backbone, we boldface the best result in the class of interpretable models.

CNN Model	ACC	Transformer Model	ACC
ResNet-34	73.3%	ViT-B/16	81.1%
↳ InfoDisent	64.1%	↳ InfoDisent	79.2%
-----	-----	-----	-----
ResNet-50	76.1%	Swin-S	83.4%
↳ InfoDisent	67.8%	↳ InfoDisent	81.4%
-----	-----	-----	-----
DenseNet-121	74.4%	MaxVit	83.4%
↳ InfoDisent	66.6%	↳ InfoDisent	83.3%
-----	-----	-----	-----
ConvNeXt-L	84.1%		
↳ InfoDisent	82.8%		

Table 3: Classification accuracy (ACC) on ImageNet dataset by competing approaches using different CNN backbones.

2022). Given that current prototype models did not perform well on the ImageNet dataset and thus lack evaluation results, Table 3 presents a comparison between the classical models and our approach.

Typically, prototype models exhibit lower performance on more complex datasets compared to traditional models. However, as shown in Table 3, our approach not only matches the performance of these classical models but also offers enhanced explainability.

**Multi-dimensional analysis** In the last experiment, we utilized the FunnyBirds (Hesse, Schaub-Meyer, and Roth 2023) dataset to evaluate our approach. The FunnyBirds dataset, along with our novel automatic evaluation protocols, supports semantically meaningful image interventions, such

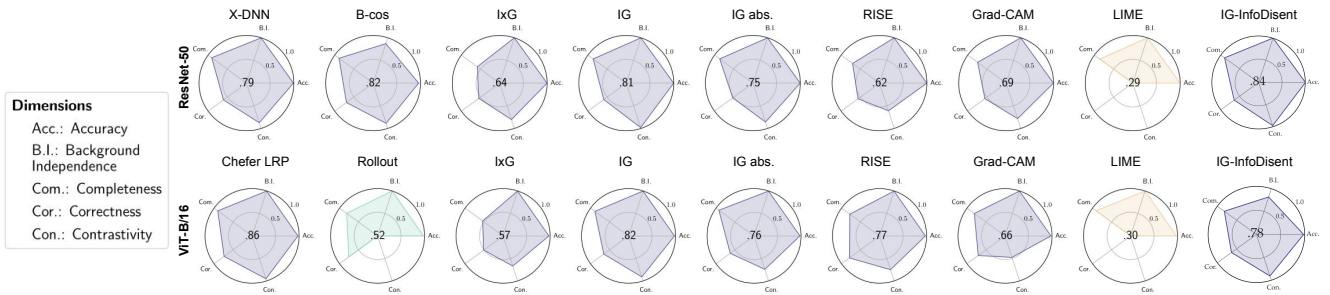


Figure 7: FunnyBirds evaluation results for various XAI methods, including Input×Gradient (IxG) (Shrikumar et al. 2016), (absolute) Integrated Gradients (IG (abs.)) (Sundararajan, Taly, and Yan 2017), Grad-CAM (Selvaraju et al. 2017), RISE (Petsiuk, Das, and Saenko 2018), LIME (Ribeiro, Singh, and Guestrin 2016), Rollout (Abnar and Zuidema 2020), Chefer LRP (Chefer, Gur, and Wolf 2021), X-DNN (Hesse, Schaub-Meyer, and Roth 2021), and B-cos (Böhle, Fritz, and Schiele 2022) network. Model-agnostic methods are assessed on ResNet-50 and ViT-B/16. Results are averaged over the entire test set, including the center score representing the mean of completeness (Com.), correctness (Cor.), and contrastivity (Con.) dimensions. Additionally, accuracy (Acc.) and background independence (B.I.) are reported. Our approach (at the end on the left) enhances model explainability, showing significant improvements for ResNet-50 and satisfactory results for the transformer model. For further details, see (Hesse, Schaub-Meyer, and Roth 2023, Sec. 4.1).

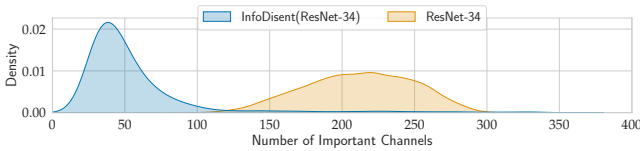


Figure 8: Density estimate of the number of significant channels for each class and image in the CUB-200-2011 test set using the ResNet-34 network. InfoDisent uses significantly fewer channels and has less variance.

as removing individual object parts. This enables a more nuanced analysis of explanations at the part level, which aligns more closely with human understanding compared to pixel-level evaluations. Results spanning a range of XAI methods and two different types of XAI model architectures are detailed in Figure 7. InfoDisent enhances the explainability of models based on classic CNN architectures like ResNet-50 and ranks among the top XAI methods for transformers.

**Ablation study** InfoDisent organizes information into channels with sparse representations, which can be later utilized in the model’s prediction process. In the following experiment, we investigate how the number of channels affects the model’s predictions. Specifically, we assess how many channels are required to account for at least 95% of the information used in the model’s predictions. Formally, if  $\text{logits} = \sum_{i=0}^N a_{ki}v_i + b_k$ , where  $N$  is a number of all channels,  $k$  represents the image class, and  $a_{ki}, v_i, b_k \in \mathbb{R}$ , then for each image from class  $k$ , we determine the smallest number  $n$  channels such that  $\sum_{i \in I_k} |a_{ki}v_i| / \sum_{i=0}^N |a_{ki}v_i| \geq 0.95$ , where  $I_k$  is the set of indexes of the  $n \leq N$  largest values of  $|a_{ki}v_i|$ . This analysis allows us to identify the most critical channels contributing to the model’s decisions, providing deeper insights into the model’s interpretability and efficiency.

Figure 8 shows the density estimate of the number of sig-

nificant channels for each class and image in the CUB-200-2011 test set. In this experiment, we used the ResNet-34 network that utilizes a significantly larger number of channels in its predictions compared to InfoDisent model. By reducing the number of significant channels while preserving classification performance, our model demonstrates efficient resource utilization and improved interpretability, as we illustrate below. This efficiency indicates that our model is more effective at isolating the critical features necessary for accurate predictions, thereby validating our approach to channel sparsity and interpretability in deep learning. This also validates the disentangling role of the orthogonal matrix  $U$ .

## Conclusions and limitations

In this paper, we introduced InfoDisent, an innovative model that integrates the strengths of both Post-hoc and inherently interpretable methods. InfoDisent offers a dual approach to interpretation by providing both local explanations (per image) and global insights (per class), thereby addressing key limitations of existing models. It builds upon the post-hoc interpretation of pre-trained networks while incorporating elements from prototypical methods, allowing for a deeper understanding of the feature space.

It should be observed that InfoDisent has some important limitations. To construct the model one needs to train the InfoDisent head on the whole dataset. The decisions of InfoDisent are formally not reduced to a small number of prototypes as in prototypical parts models. Finally, we provide interpretations to frozen feature space with InfoDisent classification head and not to the full original model.

## Supplementary Material

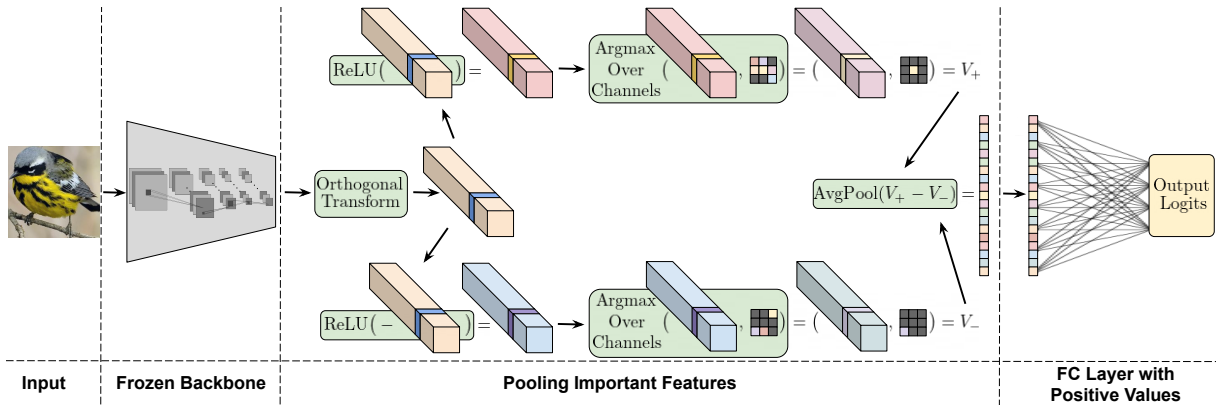


Figure 9: The architecture used for training of our proposed image classification interpretation model. InfoDisent is composed of three main components: a pre-trained backbone, a pooling layer for extracting important features, and a fully connected layer. The backbone is a pre-trained CNN or transformer with frozen weights, meaning it is not further trained. In the initial pooling layer, the model extracts representations from the last convolutional layer of the backbone and identifies key features within each channel, targeting both positive and negative activations through the application of the arg max operation. However, during training, we replace the arg max operation with the Gumbel-Softmax trick, which achieves a similar outcome in a differentiable manner. In the next step, these positive and negative features are pooled at the channel level to create a dense vector, where the vector’s dimensions correspond to the number of channels. Finally, this dense vector is passed through a fully connected linear layer with positive weights in the network’s final component.

### Architectural Adjustments for Training

In this section, we will provide a detailed explanation of the training process for the InfoDisent network. Recall that the first component of the network is the CNN or Transformer Backbone, a pre-trained classical model that is frozen up to the final feature mapping layer. During InfoDisent training, this backbone, along with its weights, remains unchanged, preserving the learned feature representations.

The second component of the network involves combining essential features from the final feature mapping produced by the Frozen Backbone. This combination mechanism encourages the network to leverage information bottlenecks, thereby constructing maximally informative and independent channels. These channels, known as prototype channels, are designed to be easily interpretable. The final component is a fully connected layer characterized by positive weight values.

To maximize the extraction of information from these channels, we introduce an information bottleneck within our model architecture. This is achieved by applying the arg max operation to individual channels, see Figure 9. While the arg max function can be used to extract a sparse representation from feature maps, our goal is to enable the model to learn to select the most important values. To achieve this, we require a differentiable arg max function. The ideal solution for this is the Gumbel-Softmax estimator (Jang, Gu, and Poole 2016). Given  $x = (x_1, \dots, x_D) \in \mathbb{R}^D$  and  $\tau \in (0, \infty)$ ,

$$\text{Gumbel-Softmax}(x, \tau) = (y_1, \dots, y_D) \in \mathbb{R}^D,$$

where

$$y_i = \frac{\exp((x_i + \eta_i)/\tau)}{\sum_{d=1}^D \exp((x_d + \eta_d)/\tau)},$$

and  $\eta_d$  for  $d \in \{1, \dots, D\}$  are samples taken from the standard Gumbel distribution.

The Gumbel-Softmax distribution serves as an interpolation between continuous categorical densities and discrete one-hot encoded categorical distributions, with the discrete form being approached as the temperature  $\tau$  decreases within the range of  $[0.1, 0.5]$ . In our experiments, we initialized  $\tau$  at 1 and progressively reduced it to 0.2. Finally, at the end of the training, we applied a hard softmax.

Following the extraction of key features using the sparse operation – specifically, the arg max operation via the Gumbel-Softmax trick – we preserve the original structure of the network’s output, maintaining the classical form of the convolutional network’s output, as shown in Figure 9. During the subsequent aggregation of positive and negative features, we utilize an average pooling operation to consolidate the information. This approach ensures that the pooled features capture a balanced representation of the activations, contributing to a robust final output.

### Details of the experiments performed

**Datasets** In our experiments, we leveraged several diverse datasets to evaluate performance. The first dataset is the Caltech-UCSD Birds-200-2011 (CUB-200-2011)(Wah et al. 2011), which contains 11,788 images meticulously labeled across 200 bird species, divided into 200 subcategories. Of these, 5,994 images are allocated for training, while 5,794



are reserved for testing. The second dataset, known as Stanford Cars (Krause et al. 2013), is designed to classify various car models. It includes 16,185 images, each capturing a rear view of different car types across 196 classes, with an almost even distribution between training (8,144 images) and testing (8,041 images) subsets. Each class details the car’s make, model, and year. The third dataset, Stanford Dogs (Khosla et al. 2011), features a collection of 20,580 images representing 120 dog breeds from around the globe. This dataset, sourced and annotated through ImageNet, is intended for fine-grained image classification, with 12,000 images for training and the remainder for testing.

Additionally, we incorporated the FunnyBirds (Hesse, Schaub-Meyer, and Roth 2023) dataset, consisting of 50,500 images representing 50 synthetic bird species, with 50,000 images for training and 500 for testing. This dataset was designed with a focus on “concepts,” or mental representations crucial for categorization, and is particularly relevant for explainable AI (XAI). The concepts are linked to specific bird anatomy parts, such as the beak, wings, feet, eyes, and tail, ensuring they are both granular and intuitive for practical use in XAI.

Finally, we utilized ImageNet (Russakovsky et al. 2015), a highly recognized dataset in computer vision, often employed for pretraining deep learning models. ImageNet encompasses 1,281,167 training images, 50,000 validation images, and 100,000 test images, spanning 1,000 object classes.

**Training Details** We train the architectures using stochastic gradient descent (SGD) with standard categorical cross-entropy loss. The momentum, damping, and weight decay are set to 0.9, 0.9, and 0.001, respectively. For the baseline networks, the initial learning rates are 0.1, 0.05, and 0.01, which are reduced by a factor of 0.1 when the validation loss converges. In our approach, we train only the last two segments of the network, thus we use lower learning rates of 0.001 and 0.0001, utilizing the ‘ReduceLROnPlateau’ (Al-Kabaji, Bensaali, and Dakua 2022) mechanism that reduces the learning rate when the cost function stops improving. All numerical experiments were conducted using NVIDIA RTX 4090 and NVIDIA A100 40 GB graphics cards.

For cropped images, we follow previous studies (Chen et al. 2019) by applying on-the-fly data augmentations (e.g., random rotation, skew, shear, and left-right flip) on the cropped CUB and cropped Cars datasets using the provided bounding boxes. We also validate our method on the full (uncropped) CUB and Dogs datasets, employing the same on-line data augmentation techniques (e.g., random affine transformation and left-right flip). For the FunnyBirds dataset, we adhered to the detailed instructions provided in the framework’s documentation, which can be found at <https://github.com/visinf/funnybirds>. For training various CNN and transformer models on the ImageNet dataset, we utilized the augmentation techniques described at <https://github.com/pytorch/vision/tree/main/references/classification>.

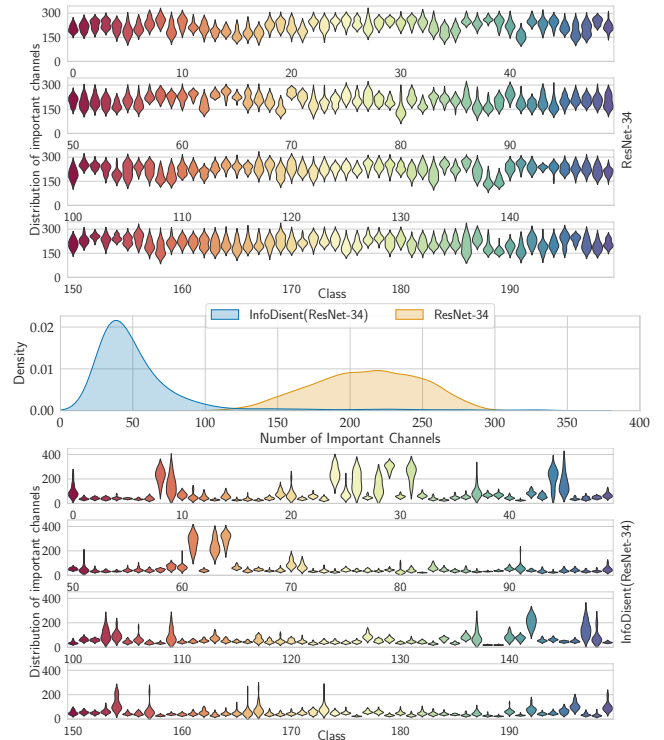


Figure 10: Density estimate of the number of significant channels for each class and image in the CUB-200-2011 test set using the ResNet-34 network. InfoDisent uses significantly fewer channels, particularly evident in the middle image, which shows the density estimation of the number of significant channels for all classes.

## Additional results

In this section, we provide additional results to supplement and expand upon the findings presented in the main part of the paper. We delve deeper into the behavior of our model across various experiments and datasets, offering a more comprehensive analysis.

**Ablation study** In this part, we present additional results from a series of analyses investigating the significance of the number of channels on model predictions across various datasets and models. The results of these analyses are illustrated in Figures 10 to 13. Recall, that InfoDisent model organizes information into channels with sparse representations, which are later utilized in the model’s prediction process. We specifically examine how the number of channels influences the model’s predictions by determining the minimum number of channels required to account for at least 95% of the information used in the model’s predictions.

Formally, if

$$\text{logits} = \sum_{i=0}^N a_{ki} v_i + b_k,$$

where  $N$  is the total number of channels,  $k$  represents the image class, and  $a_{ki}, v_i, b_k \in \mathbb{R}$ , then for each image from

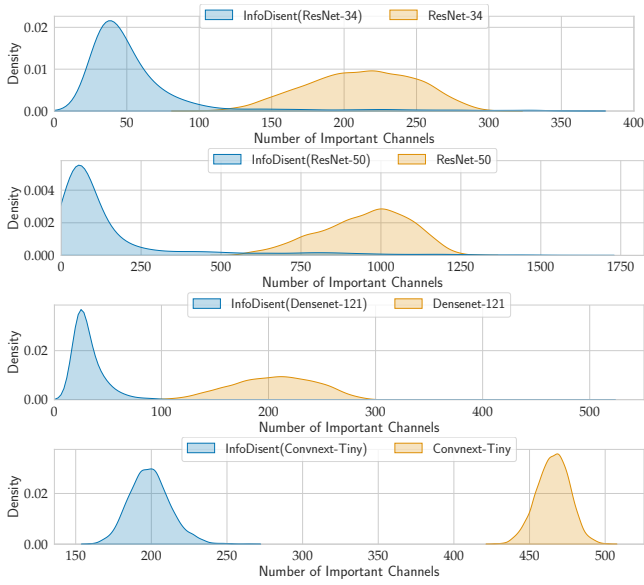


Figure 11: Density estimate of the number of significant channels for each class and image in the CUB-200-2011 test set using various networks.

class  $k$ , we identify the smallest number  $n$  of channels such that

$$\frac{\sum_{i \in I_k} |a_{ki} v_i|}{\sum_{i=0}^N |a_{ki} v_i|} \geq 0.95,$$

where  $I_k$  is the set of indexes of the  $n \leq N$  largest values of  $|a_{ki} v_i|$ .

This analysis highlights the most critical channels contributing to the model’s decisions, providing deeper insights into the model’s interpretability and efficiency. Note that the InfoDisent approach consistently utilizes significantly fewer channels, a trend observed across all models and datasets analyzed.

Figures 14 and 15 also present the channel values before the final linear layer in our model for randomly selected images from various datasets and models. As evident from the images, our model utilizes a significantly smaller number of channels in its predictions compared to the baseline models.

**Explaining Classification Decision for a Given Image by Prototypes** InfoDisent employs prototypes, similar to the approach used in PiPNet (Nauta et al. 2023a), to explain individual decisions made on an image. Below, we describe the process for identifying prototypes for a given input image. An average pooling operation makes the aggregation of information from individual channels. The outcome of this operation is a scalar for each channel  $K$ , computed as

$$\text{mx\_pool}(K) = \max(\text{ReLU}(K)) - \max(\text{ReLU}(-K))$$

(as explained in the main paper). This dense representation, formed by aggregating all the channels, is then processed by a linear layer that outputs logits, see Figure 9. The logits can be represented in a format similar to the output of a convolutional layer, as illustrated by  $V_+$  and  $V_-$  in Figure 9.

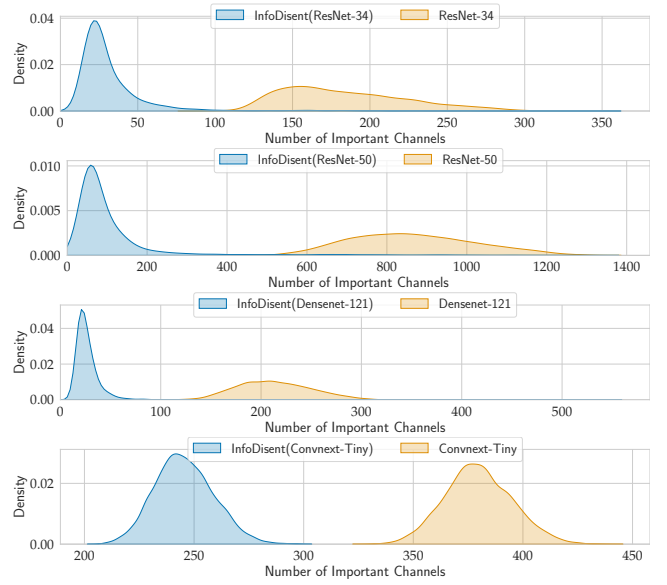


Figure 12: Density estimate of the number of significant channels for each class and image in the Stanford Cars test set using various networks.

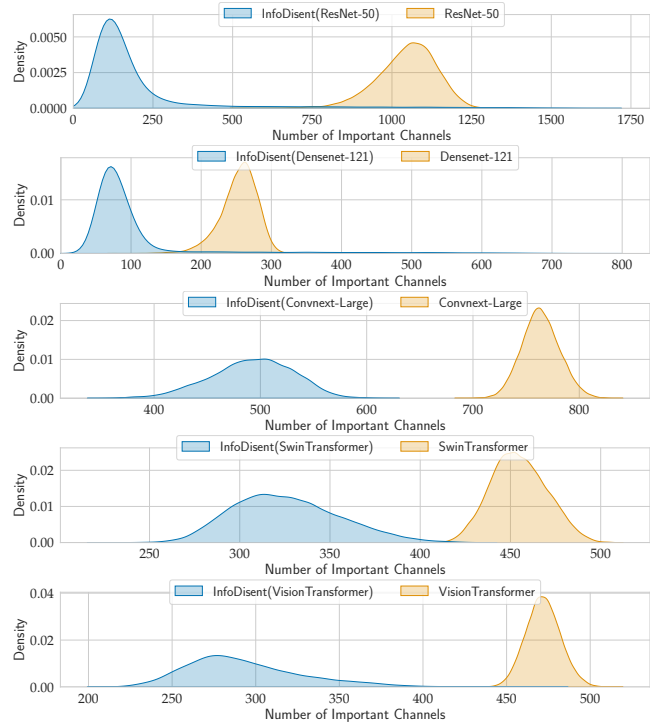


Figure 13: Density estimate of the number of significant channels for each class and image in the ImageNet test set using various networks.

This approach maintains the pictorial structure of the logits, allowing us to extract individual channels.

Note that each channel in InfoDisent model can contain only two possible values (refer to Figure 5a in the main pa-

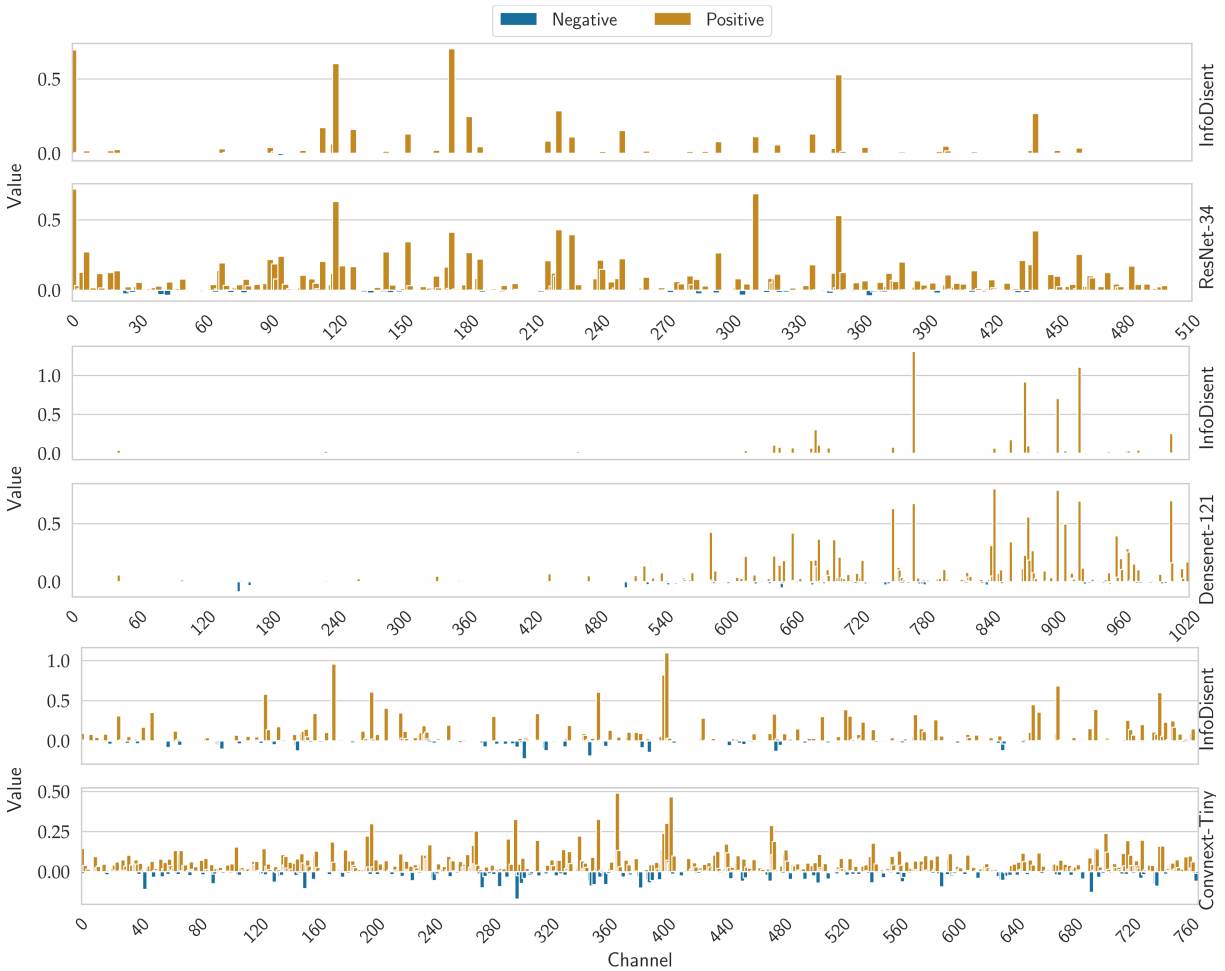


Figure 14: Channel activations before the final linear layer for a randomly selected image processed by different models trained on the CUB-200-2011 dataset are shown. The results are displayed in three groups, each containing two graphs. Model names are listed on the right side of the graphs. Unlike the baseline models, our network activates significantly fewer channels while still maintaining strong performance.

per, where these values are depicted as red or blue areas within the channels). To identify the prototype, i.e., the relevant channel, we focus solely on the positive values within the channels (represented by red areas in Figure 5a). These positive values indicate the significant part of the channel/prototype (marked by the yellow frame on the prototype) and define the channel’s importance for the model prediction (since the linear layer uses only nonnegative coefficients). As demonstrated in Figures 14 and 15, the number of such channels is limited (alternatively, we could also focus on channels with the strongest values). Once we have identified the important channels (by knowing their indices), we represent each channel using prototypes. Prototypes are images from the training set that exhibit the five strongest positive values for a given channel. Example results illustrating how model predictions are explained using prototypes are shown in Figures 16 to 20 (which are after the references).

Figures 16 to 18 showcase the performance of our prototype models on standard benchmarks: CUB-200-2011,

Stanford Cars, and Stanford Dogs. Figure 16 demonstrates the model’s ability to focus on distinctive features like the Scissor-tailed Flycatcher’s elongated tail feathers, underlying yellow coloration, or the Red-legged Kittiwake’s red feet.

Similarly, Figure 17 highlights the model’s capacity to identify key vehicle components. For instance, it accurately pinpoints the fender, bumper, and body of a Jeep Wrangler SUV 2012, and the characteristic stripes on a Ford GT Coupe 2006.

Complementing our experiments with widely used CNN models, we investigated the performance of transformer architectures, specifically VisionTransformer (ViT-B/16) (Dosovitskiy et al. 2020), SwinTransformer (Swin-S) (Liu et al. 2022a). Their results are visualized in Figures 19 and 20. Our analysis reveals that transformer models concentrate on smaller image regions than CNNs. Nevertheless, both model types generate interpretable prototypes that offer insights into the input image content.

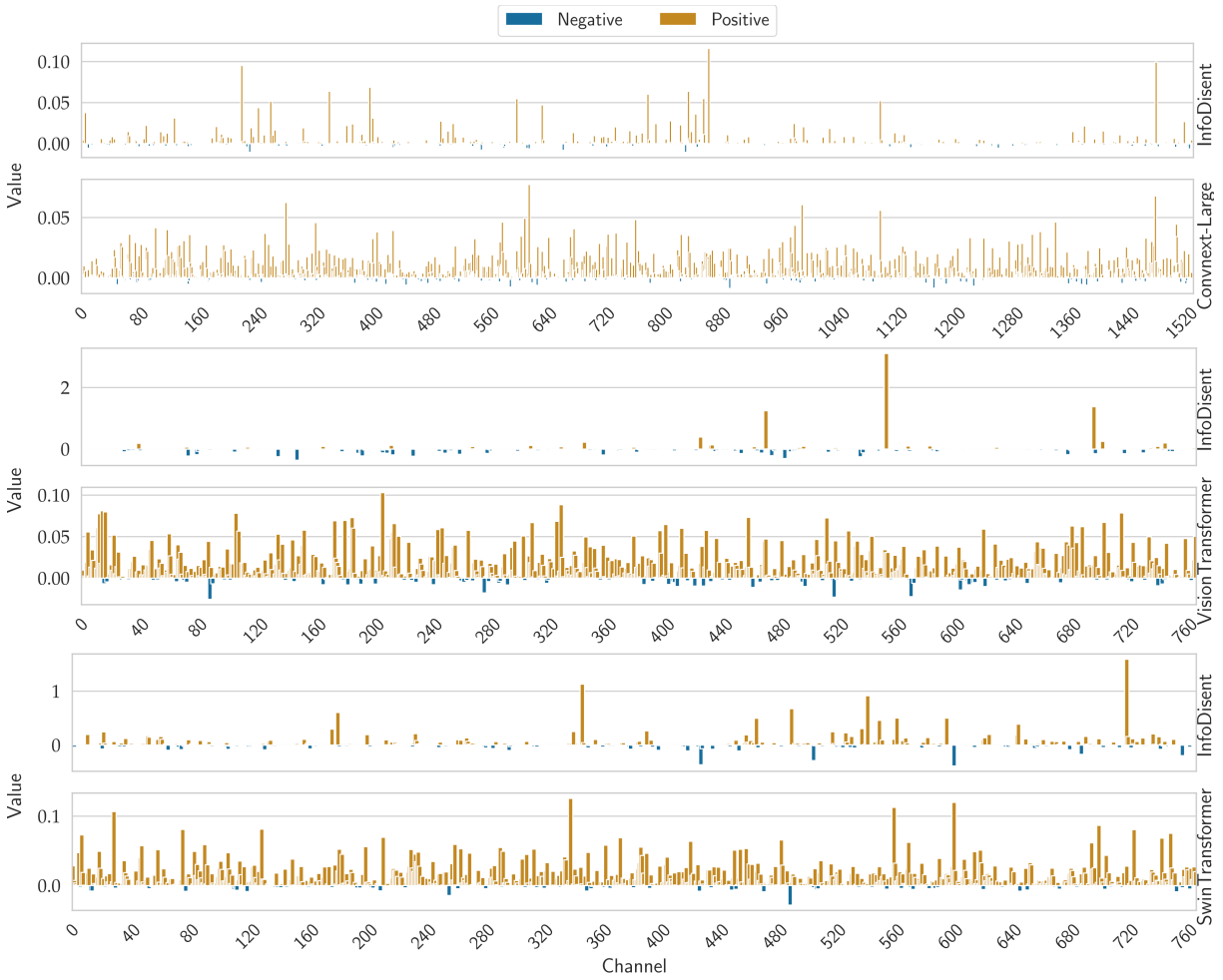


Figure 15: Channel activations before the final linear layer for a random image processed through various ConvNeXt, Vision Transformer, and Swin Transformer models trained on ImageNet. The results are displayed in three groups, each containing two graphs. Model names are listed on the right side of the graphs. InfoDisent activates significantly fewer channels compared to the baseline models while maintaining high effectiveness.

**Decision Behind Class** To delve deeper into the model’s decision-making process, we employ a prototype-based analysis at the class level. For each class, we identify key channels that consistently exhibit strong activation across the entire test set. These channels, indicative of the model’s focus on specific visual features, are selected based on their prominence and reliability in representing the class. By visualizing these key channels as prototypes, as demonstrated in our previous image analysis, we obtain a clear representation of the model’s class-specific decision criteria.

Figures 21 to 23 present the results of our prototype analysis for selected classes in the CUB-200-2011 and Stanford Cars datasets, using both InfoDisent(ResNet-50) and transformer models. This visualization allows for a granular understanding of how these models differentiate between various classes, highlighting the underlying patterns recognized by the network.

**Heatmaps** Figures 24 and 25 present example heatmaps generated by our model, resembling those produced by Grad-CAM (Selvaraju et al. 2017). Our method, rooted in representational channels, simplifies heatmap generation by accumulating activations from all prototypes (positive and negative) across all channels. Leveraging the information bottleneck principle, our approach yields more focused heatmaps compared to traditional methods.

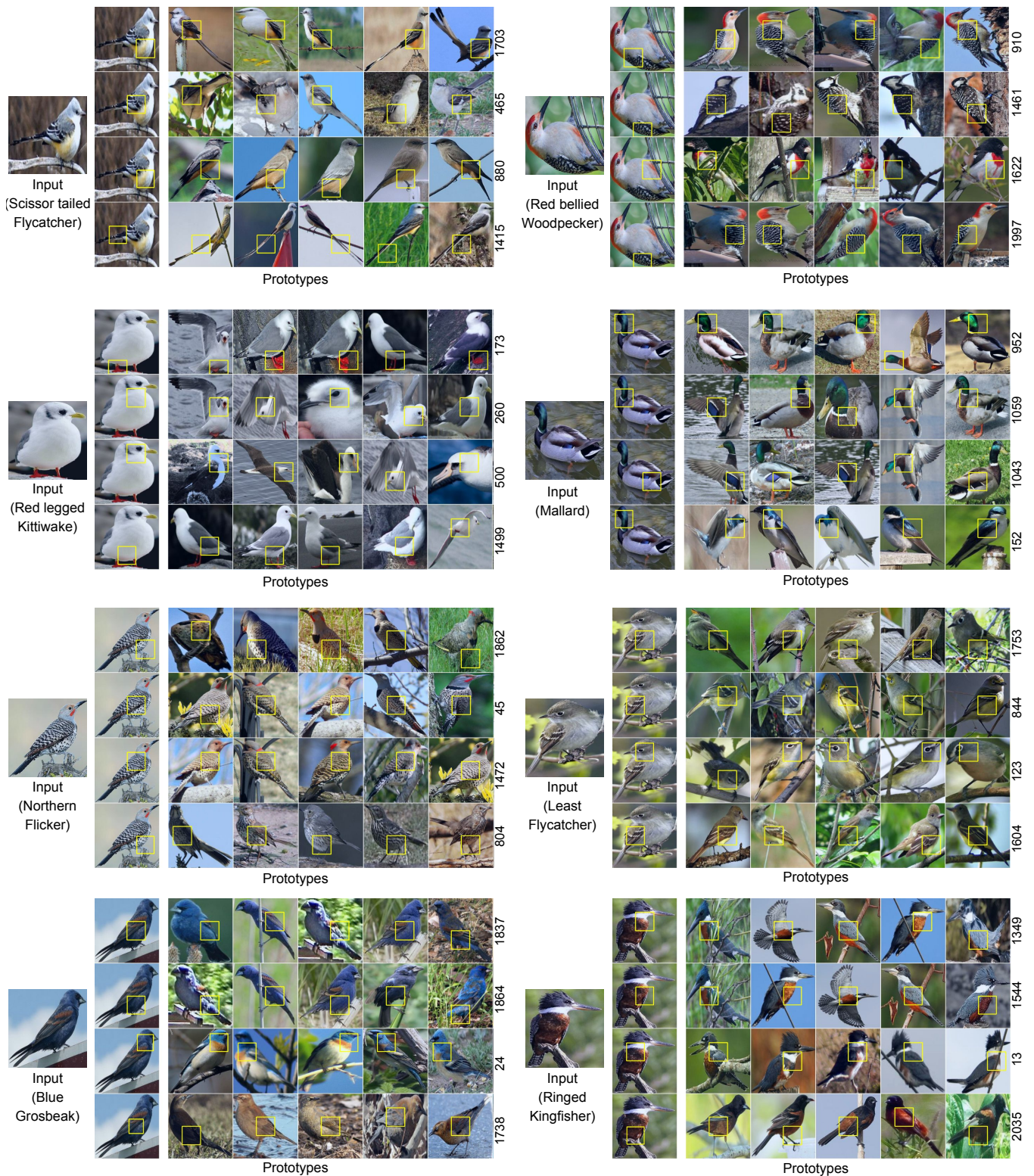


Figure 16: Example prototypes generated by InfoDisent(ResNet-50) models for random input images from the test set of the CUB-200-2011 dataset. The display includes 8 input images, each with a corresponding column where yellow boxes highlight specific regions, followed by the prototypes (images on the right). Each row represents prototypes from a different channel, with the channel index on the right. Observe that the prototypes identified by the model effectively capture distinct parts of the body in the images.



Figure 17: To demonstrate InfoDisent(ResNet-50) model's capability, we visualize prototypes generated for arbitrary test images from the Stanford Cars dataset. Each image is paired with highlighted areas and its associated prototypes, grouped by channel. The results indicate that the model has learned to extract meaningful features representing different vehicle parts.



Figure 18: Visualized prototypes from the Stanford Dogs dataset. Each row highlights prototypes from a specific channel, focusing on different dog features such as ears, nose, and fur.

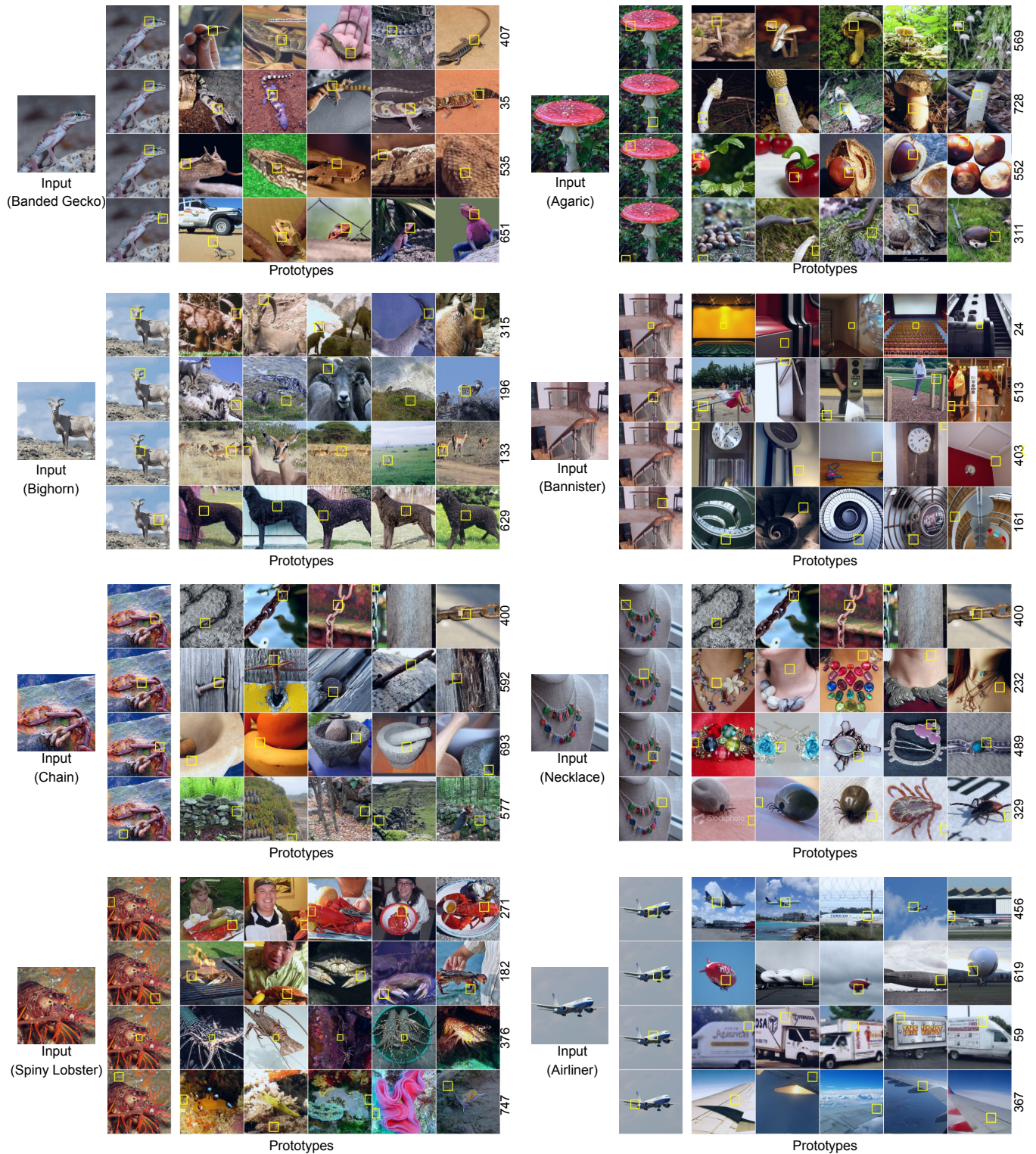


Figure 19: This figure showcases the prototypical explanations provided by InfoDisent(ViT-B/16) model. We visualize prototypes for arbitrary ImageNet images, highlighting relevant regions and their corresponding channel-specific prototypes.





Figure 20: The figure demonstrates the prototypical explainability of InfoDisent(Swin-S) model by visualizing prototypes generated for arbitrary ImageNet images, highlighting relevant image regions and their corresponding channel-specific prototypes.

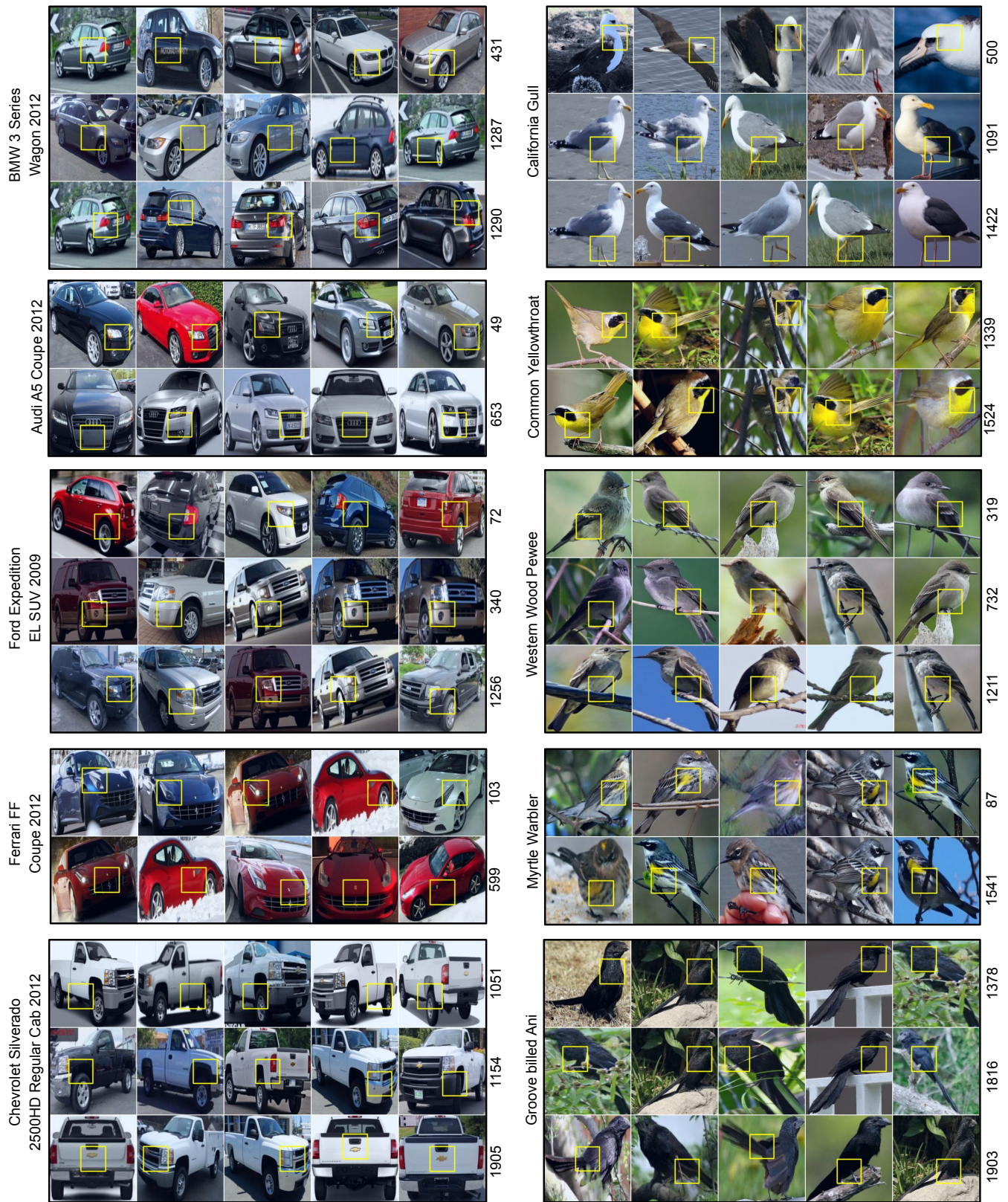


Figure 21: Prototypes of sample classes from InfoDisent(ResNet-50) model trained on the cropped Stanford Cars dataset (left) and the CUB-200-2011 dataset (right). Yellow frames highlight the class prototypes.

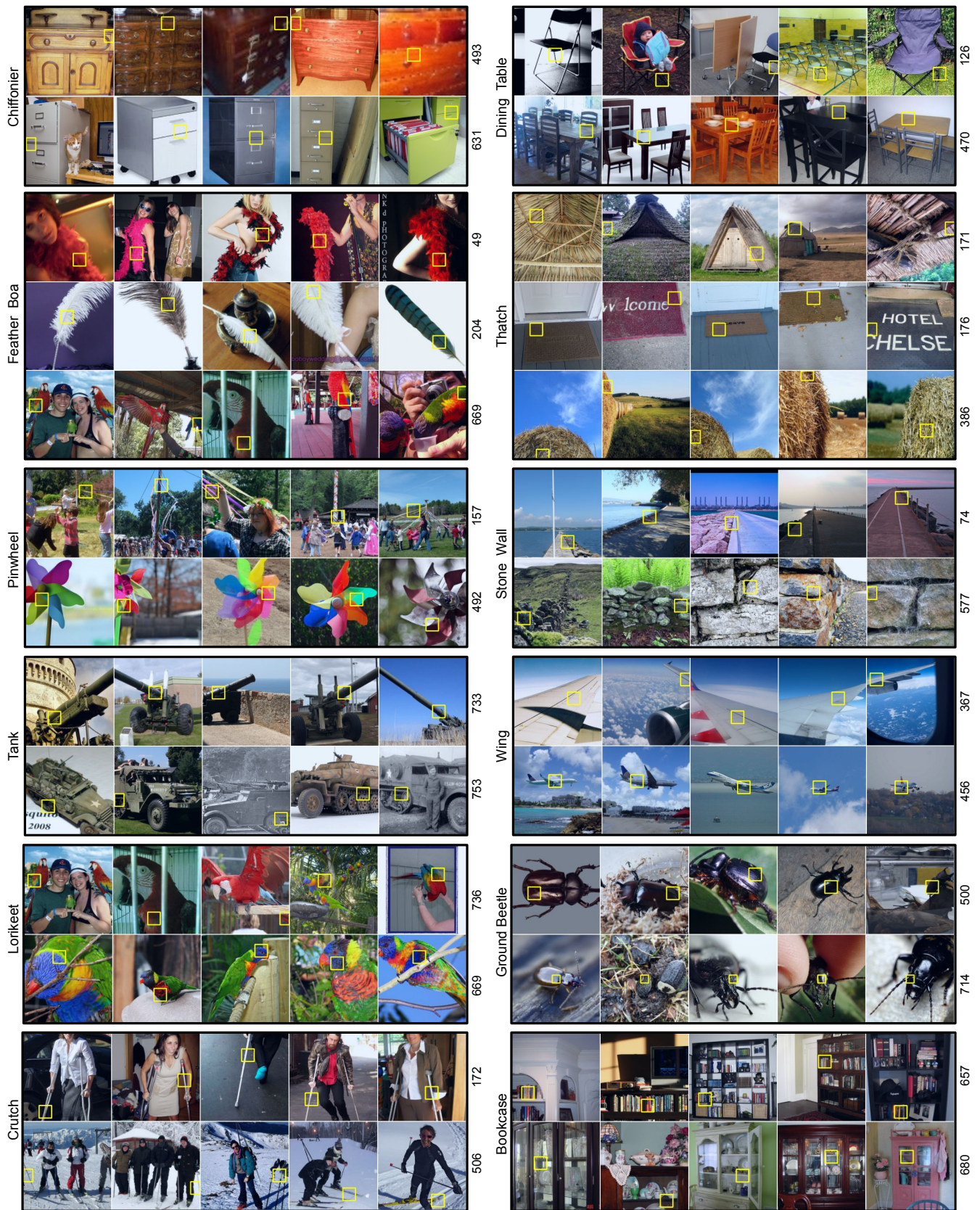


Figure 22: Visualizations of InfoDisent(ViT-B/16) model-generated prototypes for selected ImageNet categories.



Figure 23: Representative ImageNet class prototypes produced by the InfoDisent(Swin-S) model.

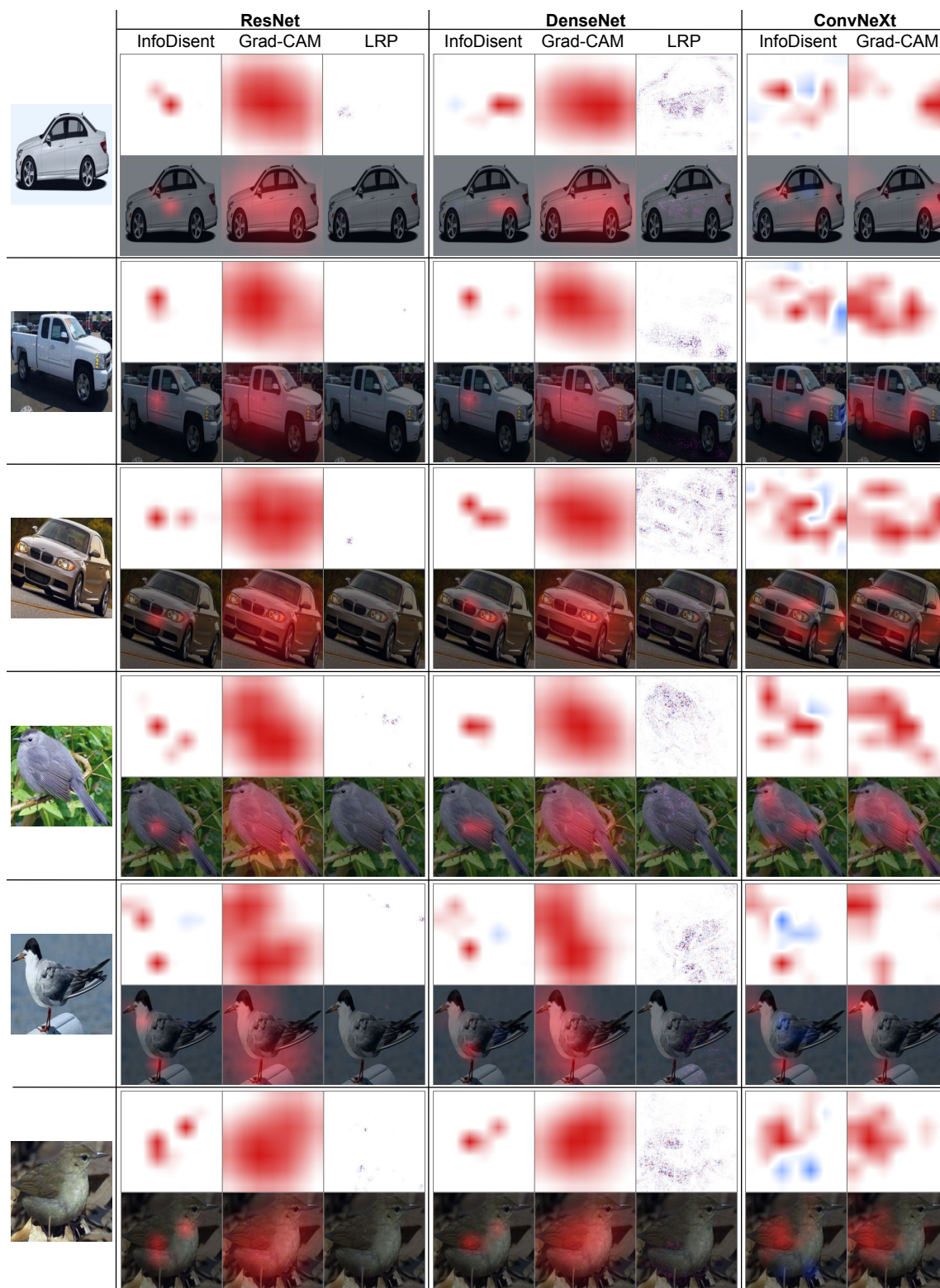


Figure 24: Comparison of example heat maps generated by InfoDisent proposed model and competing approaches. Our technique produces more focused heat maps by leveraging representational channels and the information bottleneck principle, outperforming traditional methods like Grad-CAM.

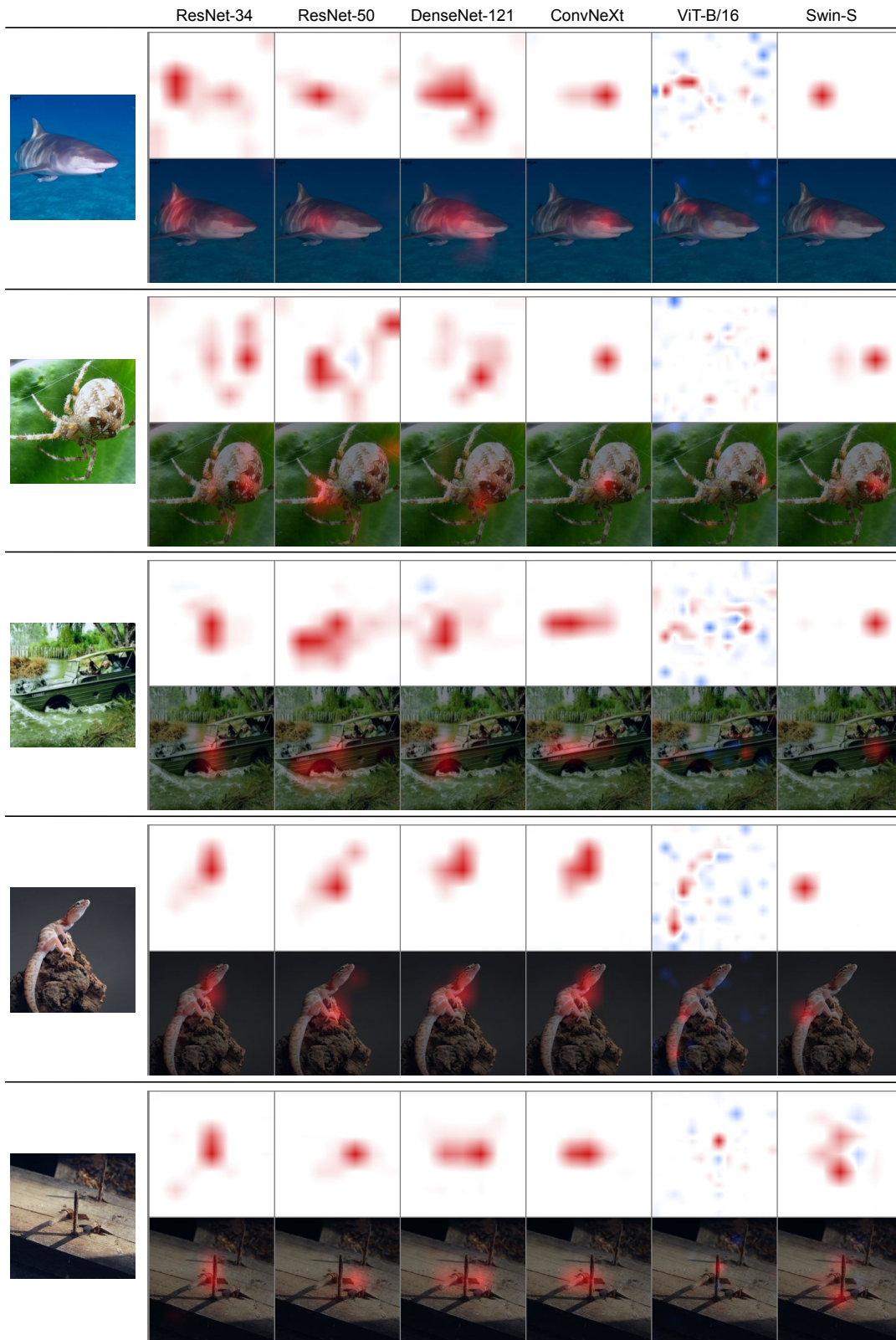


Figure 25: Example heatmaps generated by InfoDisent, our proposed method, demonstrating activation regions on sample photos from the ImageNet test set.

## References

- Abnar, S.; and Zuidema, W. 2020. Quantifying attention flow in transformers. *arXiv preprint arXiv:2005.00928*.
- Adebayo, J.; Gilmer, J.; Muelly, M.; Goodfellow, I.; Hardt, M.; and Kim, B. 2018. Sanity Checks for Saliency Maps. In *Advances in Neural Information Processing Systems*, volume 31. Curran Associates, Inc.
- Al-Kababji, A.; Bensaali, F.; and Dakua, S. P. 2022. Scheduling techniques for liver segmentation: Reducelron-plateau vs onecyclelr. In *International Conference on Intelligent Systems and Pattern Recognition*, 204–212. Springer.
- Alvarez Melis, D.; and Jaakkola, T. 2018. Towards Robust Interpretability with Self-Explaining Neural Networks. In *Advances in Neural Information Processing Systems*, volume 31. Curran Associates, Inc.
- Bach, S.; Binder, A.; Montavon, G.; Klauschen, F.; Müller, K.-R.; and Samek, W. 2015. On pixel-wise explanations for non-linear classifier decisions by layer-wise relevance propagation. *PLoS one*, 10(7): e0130140.
- Böhle, M.; Fritz, M.; and Schiele, B. 2022. B-cos networks: Alignment is all we need for interpretability. In *Proceedings of the IEEE/CVF Conference on Computer Vision and Pattern Recognition*, 10329–10338.
- Bojarski, M.; Yeres, P.; Choromanska, A.; Choromanski, K.; Firner, B.; Jackel, L.; and Muller, U. 2017. Explaining how a deep neural network trained with end-to-end learning steers a car. *arXiv preprint arXiv:1704.07911*.
- Brendel, W.; and Bethge, M. 2019. Approximating CNNs with Bag-of-local-Features models works surprisingly well on ImageNet. In *International Conference on Learning Representations*.
- Chefer, H.; Gur, S.; and Wolf, L. 2021. Transformer interpretability beyond attention visualization. In *Proceedings of the IEEE/CVF conference on computer vision and pattern recognition*, 782–791.
- Chen, C.; Li, O.; Tao, D.; Barnett, A.; Rudin, C.; and Su, J. K. 2019. This looks like that: deep learning for interpretable image recognition. *Advances in neural information processing systems*, 32.
- Donnelly, J.; Barnett, A. J.; and Chen, C. 2022. Deformable protopnet: An interpretable image classifier using deformable prototypes. In *Proceedings of the IEEE/CVF conference on computer vision and pattern recognition*, 10265–10275.
- Dosovitskiy, A.; Beyer, L.; Kolesnikov, A.; Weissenborn, D.; Zhai, X.; Unterthiner, T.; Dehghani, M.; Minderer, M.; Heigold, G.; Gelly, S.; et al. 2020. An image is worth 16x16 words: Transformers for image recognition at scale. *arXiv preprint arXiv:2010.11929*.
- Guidotti, R.; Monreale, A.; Matwin, S.; and Pedreschi, D. 2020. Explaining Image Classifiers Generating Exemplars and Counter-Exemplars from Latent Representations. *Proceedings of the AAAI Conference on Artificial Intelligence*, 34(09): 13665–13668.
- Hall, B. C.; and Hall, B. C. 2013. *Lie groups, Lie algebras, and representations*. Springer.
- He, K.; Zhang, X.; Ren, S.; and Sun, J. 2016. Deep residual learning for image recognition. In *Proceedings of the IEEE conference on computer vision and pattern recognition*, 770–778.
- Hesse, R.; Schaub-Meyer, S.; and Roth, S. 2021. Fast axiomatic attribution for neural networks. *Advances in Neural Information Processing Systems*, 34: 19513–19524.
- Hesse, R.; Schaub-Meyer, S.; and Roth, S. 2023. Funny-Birds: A synthetic vision dataset for a part-based analysis of explainable AI methods. In *Proceedings of the IEEE/CVF International Conference on Computer Vision*, 3981–3991.
- Huang, G.; Liu, Z.; Van Der Maaten, L.; and Weinberger, K. Q. 2017. Densely connected convolutional networks. In *Proceedings of the IEEE conference on computer vision and pattern recognition*, 4700–4708.
- Jang, E.; Gu, S.; and Poole, B. 2016. Categorical reparameterization with gumbel-softmax. *arXiv:1611.01144*.
- Khan, J.; Wei, J. S.; Ringner, M.; Saal, L. H.; Ladanyi, M.; Westermann, F.; Berthold, F.; Schwab, M.; Antonescu, C. R.; Peterson, C.; et al. 2001. Classification and diagnostic prediction of cancers using gene expression profiling and artificial neural networks. *Nature medicine*, 7(6): 673–679.
- Khosla, A.; Jayadevaprakash, N.; Yao, B.; and Li, F.-F. 2011. Novel dataset for fine-grained image categorization: Stanford dogs. In *Proc. CVPR workshop on fine-grained visual categorization (FGVC)*, volume 2.
- Krause, J.; Stark, M.; Deng, J.; and Fei-Fei, L. 2013. 3d object representations for fine-grained categorization. In *Proceedings of the IEEE international conference on computer vision workshops*, 554–561.
- Liu, N.; Zhang, N.; Wan, K.; Shao, L.; and Han, J. 2021. Visual saliency transformer. In *Proceedings of the IEEE/CVF International Conference on Computer Vision*, 4722–4732.
- Liu, Z.; Hu, H.; Lin, Y.; Yao, Z.; Xie, Z.; Wei, Y.; Ning, J.; Cao, Y.; Zhang, Z.; Dong, L.; et al. 2022a. Swin transformer v2: Scaling up capacity and resolution. In *Proceedings of the IEEE/CVF conference on computer vision and pattern recognition*, 12009–12019.
- Liu, Z.; Mao, H.; Wu, C.-Y.; Feichtenhofer, C.; Darrell, T.; and Xie, S. 2022b. A convnet for the 2020s. In *Proceedings of the IEEE/CVF conference on computer vision and pattern recognition*, 11976–11986.
- Lundberg, S. M.; and Lee, S.-I. 2017. A unified approach to interpreting model predictions. *Advances in neural information processing systems*, 30.
- Nauta, M.; Schlötterer, J.; van Keulen, M.; and Seifert, C. 2023a. PIP-Net: Patch-Based Intuitive Prototypes for Interpretable Image Classification.
- Nauta, M.; Trienes, J.; Pathak, S.; Nguyen, E.; Peters, M.; Schmitt, Y.; Schlötterer, J.; Van Keulen, M.; and Seifert, C. 2023b. From anecdotal evidence to quantitative evaluation methods: A systematic review on evaluating explainable ai. *ACM Computing Surveys*, 55(13s): 1–42.
- Patrício, C.; Neves, J. C.; and Teixeira, L. F. 2023. Explainable deep learning methods in medical image classification: A survey. *ACM Computing Surveys*, 56(4): 1–41.

- Petsiuk, V.; Das, A.; and Saenko, K. 2018. Rise: Randomized input sampling for explanation of black-box models. *arXiv preprint arXiv:1806.07421*.
- Ribeiro, M. T.; Singh, S.; and Guestrin, C. 2016. "Why should i trust you?" Explaining the predictions of any classifier. In *Proceedings of the 22nd ACM SIGKDD international conference on knowledge discovery and data mining*, 1135–1144.
- Russakovsky, O.; Deng, J.; Su, H.; Krause, J.; Satheesh, S.; Ma, S.; Huang, Z.; Karpathy, A.; Khosla, A.; Bernstein, M.; et al. 2015. Imagenet large scale visual recognition challenge. *International journal of computer vision*, 115: 211–252.
- Rymarczyk, D.; Struski, Ł.; Górszczak, M.; Lewandowska, K.; Tabor, J.; and Zieliński, B. 2022. Interpretable image classification with differentiable prototypes assignment. In *European Conference on Computer Vision*, 351–368. Springer.
- Rymarczyk, D.; Struski, Ł.; Tabor, J.; and Zieliński, B. 2021. Protoshare: Prototypical parts sharing for similarity discovery in interpretable image classification. In *Proceedings of the 27th ACM SIGKDD Conference on Knowledge Discovery & Data Mining*, 1420–1430.
- Samek, W.; Montavon, G.; Lapuschkin, S.; Anders, C. J.; and Müller, K.-R. 2021. Explaining deep neural networks and beyond: A review of methods and applications. *Proceedings of the IEEE*, 109(3): 247–278.
- Selvaraju, R. R.; Cogswell, M.; Das, A.; Vedantam, R.; Parikh, D.; and Batra, D. 2017. Grad-cam: Visual explanations from deep networks via gradient-based localization. In *Proceedings of the IEEE international conference on computer vision*, 618–626.
- Shapley, L. S. 1951. Notes on the n-person game-ii: The value of an n-person game.
- Shepard, R.; Brozell, S. R.; and Gidofalvi, G. 2015. The representation and parametrization of orthogonal matrices. *The Journal of Physical Chemistry A*, 119(28): 7924–7939.
- Shrikumar, A.; Greenside, P.; Shcherbina, A.; and Kundaje, A. 2016. Not just a black box: Learning important features through propagating activation differences. *arXiv preprint arXiv:1605.01713*.
- Struski, Ł.; Janusz, S.; Tabor, J.; Markiewicz, M.; and Lewicki, A. 2024. Multiple instance learning for medical image classification based on instance importance. *Biomedical Signal Processing and Control*, 91: 105874.
- Sundararajan, M.; Taly, A.; and Yan, Q. 2017. Axiomatic attribution for deep networks. In *International conference on machine learning*, 3319–3328. PMLR.
- Tu, Z.; Talebi, H.; Zhang, H.; Yang, F.; Milanfar, P.; Bovik, A.; and Li, Y. 2022. Maxvit: Multi-axis vision transformer. In *European conference on computer vision*, 459–479. Springer.
- Wah, C.; Branson, S.; Welinder, P.; Perona, P.; and Belongie, S. 2011. The caltech-ucsd birds-200-2011 dataset.
- Wang, J.; et al. 2021. Interpretable Image Recognition by Constructing Transparent Embedding Space. In *ICCV*, 895–904.
- Xu, F.; Uszkoreit, H.; Du, Y.; Fan, W.; Zhao, D.; and Zhu, J. 2019. Explainable AI: A brief survey on history, research areas, approaches and challenges. In *Natural language processing and Chinese computing: 8th CCF international conference, NLPCC 2019, dunhuang, China, October 9–14, 2019, proceedings, part II* 8, 563–574. Springer.
- Zheng, H.; Fu, J.; Zha, Z.-J.; and Luo, J. 2019. Looking for the devil in the details: Learning trilinear attention sampling network for fine-grained image recognition. In *Proceedings of the IEEE/CVF Conference on Computer Vision and Pattern Recognition*, 5012–5021.